A First Principles Analysis of the Effect of Hydrogen Concentration in Hydrogenated Amorphous Silicon on the Formation of Strained Si-Si Bonds and the Optical and Mobility Gaps

Merid Legesse, Michael Nolan and Giorgos Fagas

Tyndall National Institute, University College Cork, Lee Maltings, Dyke Parade, Cork, Ireland

Michael.nolan@tyndall.ie

Georgios.fagas@tyndall.ie

Abstract

In this paper we use a model of hydrogenated amorphous silicon generated from molecular dynamics with density functional theory calculations to examine how the atomic geometry and the optical and mobility gaps are influenced by mild hydrogen oversaturation. The optical and mobility gaps show a volcano curve as the hydrogen content varies from undersaturation to mild oversaturation, with largest gaps obtained at the saturation hydrogen concentration. At the same time, mid-gap states associated with dangling bonds and strained Si-Si bonds disappear at saturation but reappear at mild oversaturation which is consistent with the evolution of optical gap. The distribution of Si-Si bond distances provides the key to the change in electronic properties. In the undersaturation regime the new electronic states in the gap arise from the presence of dangling bonds and strained Si-Si bonds, which are longer than the equilibrium Si-Si distance. Increasing hydrogen concentration up to saturation

reduces the strained bonds and removes dangling bonds. In the case of mild oversaturation the mid-gap states arise exclusively from an increase in the density of strained Si-Si bonds. Analysis of our structure shows that the extra hydrogen atoms form a bridge between neighbouring silicon atoms, thus increasing the Si-Si distance and increasing disorder in the sample.

1. Introduction

A leading material over the last four decades in the production of thin film solar cells is hydrogenated amorphous silicon (a-Si:H) [1]. This material is also important for the realisation of cheaper electronic devices like liquid crystal displays, thin film transistors and optoelectronic devices [1, 4] and is a model system for the study of fundamental properties of amorphous and disordered materials [5]. Despite its amorphous character, which reduces carrier mobility, the primary advantage offered by a-Si:H compared to crystalline silicon (c-Si) lies in its economically favourable production technique. Thin films of a-Si:H can be deposited over large areas using plasma enhanced chemical vapor deposition at low temperatures, allowing the use of plastic and flexible substrates in a cheap roll-to-roll process [6]. In contrast, there are significant costs associated with using c-Si.

In the visible part of the solar spectrum the absorption coefficient of a-Si:H is higher by an order of magnitude than that of c-Si [7]. Higher absorption coefficient means that less material is required to absorb the same amount of light, thus allowing the use of thin films 1 μm. Although a-Si:H is a promising material for cheaper electronic devices and solar cells, there are also some fundamental disadvantages compared to c-Si. Among them, we can mention the lower carrier mobility (1 cm^2/Vs) of a-Si:H as compared to 1000 cm^2/Vs in c-Si and the serious efficiency degradation during the initial exposure to sunlight due to the well-known Staebler-Wronski effect [8]. Although this is a well studied effect, its origin remains a subject of great discussion and controversy. Recently the role of vacancies and voids in the light-induced degradation process was discussed [9-12]. In addition, the larger band gap over c-Si leads to less efficient harvesting of solar radiation. Understanding the roles of disorder, hydrogen (H) concentration and structure have aided, and continue to aid, improving the photovoltic conversion efficiency with respect to earlier devices.

As grown a-Si is a highly defective amorphous material, possessing numerous low coordinated Si atoms and Si-Si bonds and bond angles that deviate significantly from the bulk c-Si atomic geometry. A primary defect is the so-called dangling bond, which is present in a-Si when undercoordinated Si atoms are formed. Incorporation of H during a-Si:H growth, either intentionally or not, is believed to passivate these dangling bonds and break strained or weak Si-Si bonds, both of which can reduce the concentration of these defects in the system and reduce the disorder compared to unhydrogenated a-Si. [1]. However, in a grown a-Si:H film, an increase in the hydrogen content can be associated with a higher degree of disorder [13]. H concentration also strongly influences the fundamental optical and mobility gaps in a-Si:H [14]. The importance of short and long Si-Si bonds has recently been discussed in the context of the band tail and mid-gap states in a-Si:H [15-20]. The presence of band tails and mid-gap states results in very different electronic properties of a-Si:H compared to the equivalent c-Si [1,18]. The band tail states represent the energy states of electrons that are formed by the distorted bonds angle and bond length in the *a*-Si:H network. The width of the band tails is a measure of the degree of disorder in *a*-Si:H, or in any amorphous material [19]. The actual understanding is that valance band tail states are contributed from short Si-Si bonds and conduction band tail states come from long Si-Si bonds [15-17]. In addition, ref [20] shows that the strained bonds (longer Si-Si bonds) significantly contribute to the mid-gap states as much as dangling bonds.

The optical properties of a-Si:H are intimately related to changes in its structure, compositional disorder and H concentration [21-27]. The dependence of the optical gap of a-Si:H on H content, up to saturation, has been well studied [14, 21-27]. To summarise, Cody et al. [27] showed that the optical gap of a-Si:H films, $E_{opt,}$ is independent of the H concentration, so long as H saturation is achieved. By contrast, later studies [17–23] generally claimed that the optical gap of a-Si:H is dependent on H concentration, even though some of

them [18 – 21] showed that a constant optical gap is achieved at saturation. Our previous work [14] showed for the first time that the optical and mobility gaps of a-Si:H are invariant with H content as long as H saturation is reached.

In contrast to many studies, our calculations in this work are focused on the impact on a-Si:H optical and mobility gaps of a small increase (< 4 %) in the H concentration of hydrogen beyond saturation which we term **mild oversaturation** and for which we have not found any previous studies in the literature. This regime of H content is distinct to that studied in refs. [28-30], in which hypersaturation of H is used to generate nanoscopic regions of c-Si in an a-Si:H matrix. A 4 % increase in H content past saturation is chosen as it does not lead to formation of c-Si domains, permits the regime of mild oversaturation to be explored and allows us to still have a reasonable computational expense in a 512 Si atom supercell, model (which we validated against a-Si supercells with up to 4098 atoms) and allowing hybrid DFT calculations to be carried out as a check on the GGA-DFT results. In Refs. [28-30] there is a constant supply of H to a-Si:H, while in this paper we investigate a-Si:H structures with fixed H contents, which approximates a-Si:H at the end of deposition. While the addition of H to a-Si up to saturation will increase the order of the system, in the sense that defects such as dangling Si are passivated or strained Si-Si bonds are broken and passivated with hydrogen, we find that mild oversaturation with H actually results in formation of new strained Si-Si bonds, which has a profound effect on the optical and mobility gaps, with both showing a maximum at hydrogen saturation. The effect of H content on going from undersaturation to saturation and to mild oversaturation is analyzed in terms of the Si-Si bonds in the a-Si:H system and the electronic density of states, highlighting the importance of strained Si-Si bonds in determining the properties of a-Si:H.

2.0 Methods and preparation

We employ a heat and quench approach to generate models of a-Si and a-Si:H within classical molecular dynamics (MD) with the empirical Tersoff interatomic potential for Si [31-33], which has been used extensively for c-Si and a-Si [32, 33]. All MD simulations are carried out with the GULP code [34]. Different structural models have been proposed for a-Si [35, 36], including the continuous random network (CRN) model [35], where every atom has four-fold coordination, heat and quench and direct production from silane [28-30]. With experiments on pure a-Si giving an average coordination number of 3.88 and non-vanishing density of states in the gap, the CRN model lacks some consistency with experiment. In contrast, heat and quench results in formation of under coordinated Si atoms, giving three and five fold coordinated Si, that is the dangling bond and the floating bond [18, 37], and a non-zero mid-gap density of states [36] in consistency with experiments.

Our a-Si structure is generated by an initial simulation to melt a 512 atoms bulk c-Si structure at 3500 K for 250 ps in the NVT ensemble. We quench to 300 K at a rate of $1x10^{12}$ K/s and anneal for 100 ps at 600 K. Finally we relax this a-Si structure using DFT (as described below). By incorporating H into this a-Si model to passivate all under coordinated Si, we generate a model of a-Si:H, with an optimum, saturation H concentration. In our earlier work, we examined H contents of 14%, 15 % and 16.5 % [14] and in this work, we focus on saturation H content of 14 %. This saturated model structure of a-Si:H is relaxed with GGA-DFT. To examine how H content, at both under- and over-saturated regimes, affects the optical and mobility gaps, we further generate six a-Si:H structures. Four of them are undersaturated and obtained by removing H from the 14% saturated structure with H concentrations of 7%, 9%, 12%, and 13%, and the remaining two a-Si:H structures are mildly oversaturated, by adding H to the 14% saturated structure, with H concentrations of 16% and 18% H.

All structural, electronic and optical properties of a-Si:H are calculated from first-principles after performing ionic relaxations within density functional theory (DFT) [38] on the structural models obtained from the heat and quench procedure. We used the generalized gradient approximation (PW91-GGA) [39] to the exchange-correlation functional as implemented in the Vienna *ab initio* simulation package (VASP) [40]. The interaction between ion cores and valence electrons is described using the projector-augmented wave method (PAW) [41], with 4 electrons on Si and 1 electron on H. The electronic wavefunctions are described within a plane wave basis set and the kinetic-energy cutoff is set to 400 eV. Irreducible Brillouin zone integration for the supercell of 512-atoms is conducted using Γ point sampling [42]. A Gaussian smearing of width 0.05 eV is applied to determine the band occupations and electronic density of states. A concern for these calculations is the severe underestimation of the band gap with GGA-DFT which we calculate to be 0.7 eV for c-Si, compared to 1.1 eV in experiment. To address this fundamental point, further hybrid DFT calculations, using the HSE06 [43] functional, with 25% exact exchange and a screening length of 0.2 $Å^{-1}$, are performed at the GGA-DFT geometry. In this way we are able to determine more accurately the mobility gaps in our under saturated, saturated and mild oversaturated models of a-Si:H.

3. Results

3.1 Structural analysis of hydrogenated amorphous silicon with different H concentrations

The structural analysis of a-Si:H allows us to examine both the quality of the amorphous structure generated from the heat and quench procedure and any effects arising from H

content. For this analysis we obtained the distribution of Si-Si bond lengths, the radial distribution function (RDF), the vibrational density of states and the tetrahedral angle distribution. In Fig. 1 (a-c) we show a typical atomic structure for a-Si:H (with undersaturated, 7%, saturated, 14%, and mildly oversaturated, 18%, H concentrations) relaxed with GGA. In all a-Si:H structures of H is predominantly present in Si-H bonds, comprising 95% of all Si-H_n bonds, and the remainder is bonded forming Si-H_2 (4%) and Si-H_3 (1%). Si-H_n bonds have been observed experimentally from infrared spectroscopy [44]. The formation of a smaller number of Si-H_2 is an indication of high quality grade hydrogenated amorphous silicon [45]. The average coordination numbers in a-Si:H with 7%, 14 % and 18% H concentrations are 3.80, 3.92 and 4.01, respectively. Our value for saturated a-Si:H compares well with the experimental value of 3.88 for H-saturated a-Si:H [46], while the value for mild oversaturation indicates a higher concentration of 5-fold coordinated Si atoms.

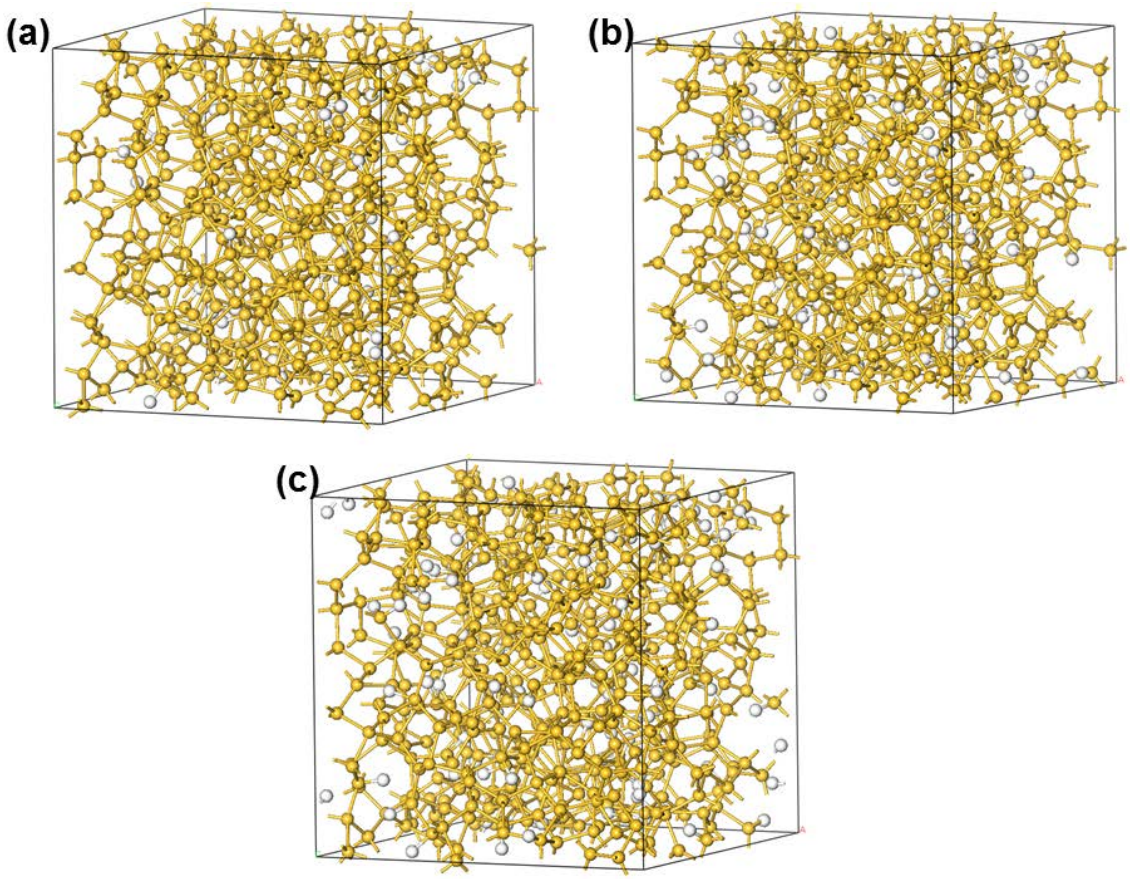

Fig. 1 Structural models for 512 Si atoms with (a) 14% H concentration in saturated a-Si: H, (b) 7% H concentration in undersaturated a-Si:H and (c) 18% H concentration in mildly over saturated a-Si: H. Si are yellow spheres and H are white spheres.

We show the Si-Si RDF as a function of H concentration in Fig. 2. In general, the RDF is typical of a-Si and a-Si:H, with a well-defined peak at the nearest neighbour Si-Si distance and broadened and flattened peaks for the remaining Si-Si distances that are characteristics due to the lack of long range order in a-Si and a-Si:H. The obtained RDF is also consistent with previous theoretical and experimental work [28-30, 46-47].

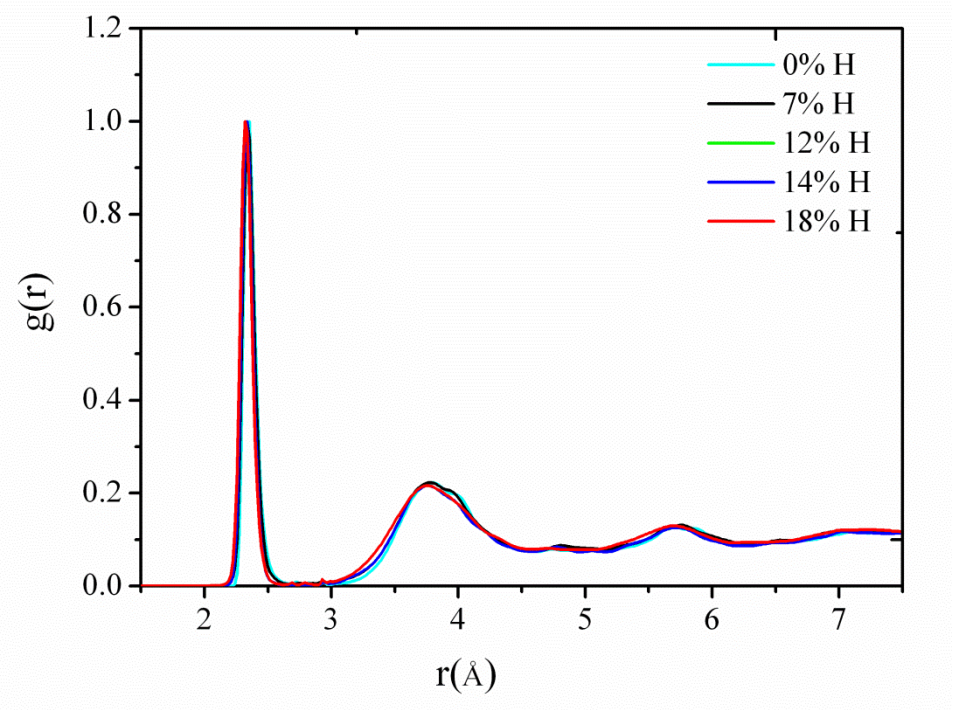

Fig. 2. Si-Si radial distribution functions in a-Si and a-Si:H for different % H contents.

To investigate the vibrational properties of a-Si and a-Si:H we compute the phonon density of states (PDOS):

$$PDOS = \frac{1}{3N}\sum_{i=1}^{3N}\delta(\omega - \omega i) \qquad (1)$$

where ω_i i = 1, 2, 3... 3N are the phonon frequencies. The *PDOS* of a-Si and for a-Si:H different H concentrations are plotted in Fig. 3. For all calculations we have found no negative frequencies, which shows that our systems are in a local minimum. As we can see from Fig. 3, the position of transverse acoustic (TA) mode, centred at 20 meV, and transverse optical (TO) mode, centred at 62 meV, are in reasonable agreement with the positions of the experimental TA and TO peaks, at 20 and 61 meV [48-49].

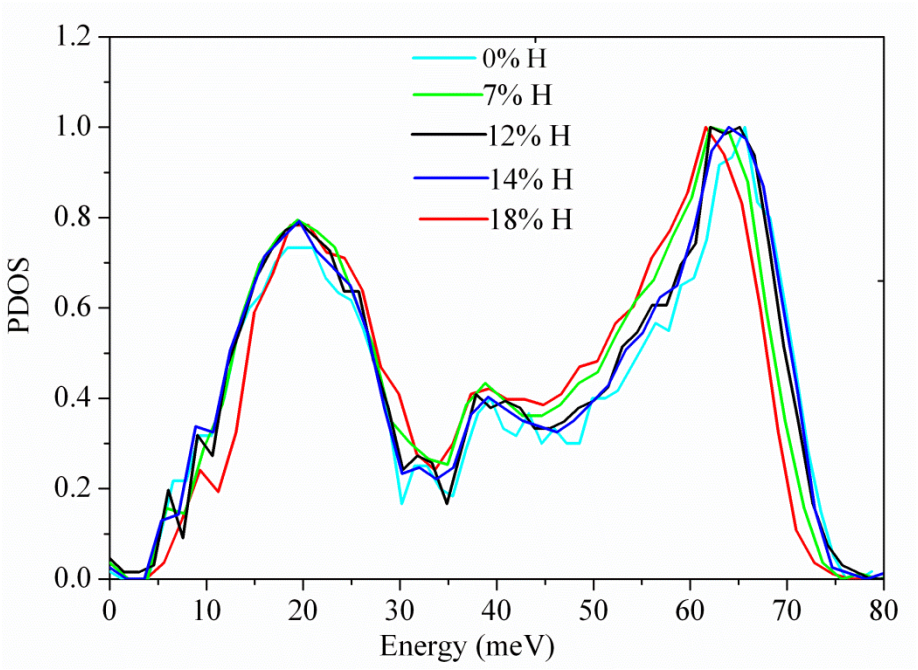

Fig. 3. Vibrational density of states for bulk a-Si and a-Si:H with different H contents.

Fig. 4 shows the distribution of Si-Si-Si tetrahedral angles for a-Si and a-Si:H with different H concentrations. The overall shape of the angle distribution is consistent with earlier works [50-51], again confirming that our models are reasonable. The peak around the crystalline Si tetrahedral angle of 109.5^{o} generally narrows as H is added to the system.

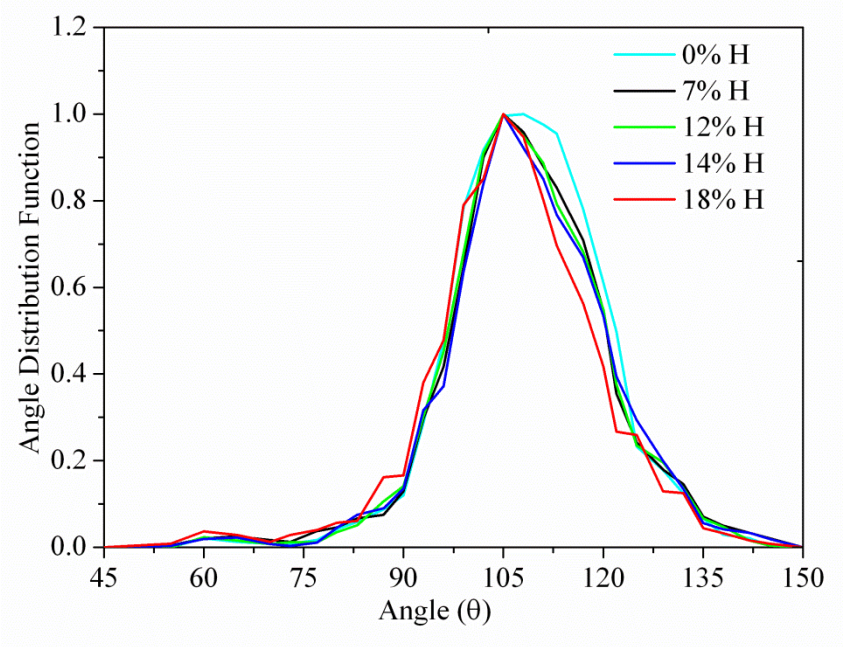

Fig. 4. Tetrahedral angle distribution for bulk a-Si and a-Si:H with different H content

3.2 Optical and Electronic Properties of hydrogenated amorphous silicon

3.2.1 Optical properties of hydrogenated amorphous silicon

The optical properties of a-Si:H are characterised by the *optical band gap*, which is important for solar cell applications since it is the fundamental quantity that characterises light absorption in the material. From the computed dielectric function, the optical band gap is determined from a Tauc plot, in which we extrapolate the linear part of the function $[\alpha(E)\times E]^{1/2}$ plotted against the photon energy E. Here $\alpha(E)$ is the absorption coefficient which is calculated from

$$\alpha = \frac{2\kappa\pi}{\lambda} \qquad (2)$$

Where λ is the free space wavelength of light and κ is the extinction coefficient. The expression for κ reads

$$\kappa = \frac{1}{\sqrt{2}}\sqrt{-\varepsilon_1 + \sqrt{{\varepsilon_1}^2 + {\varepsilon_2}^2}} \qquad (3)$$

The variables ε_1 and ε_2 represent respectively the real and imaginary part of the dielectric function of each a-Si:H structure, calculated using the VASP post-processing routines of Furthmueller [52]. Fig. 5 shows the Tauc plot from which we obtain the optical band gap of undersaturated a-Si:H with different H content [14]. We fit the linear part of each plot with a linear function and extrapolation of this function allows us to obtain the optical gap of each a-Si:H sample. We realise the limitations of this approach for fitting the optical gap of a-Si:H, however our results from ref. [14] give us confidence in using this approach to determine the optical gap and hence analyse the effect of H content on the optical gap of a-Si:H

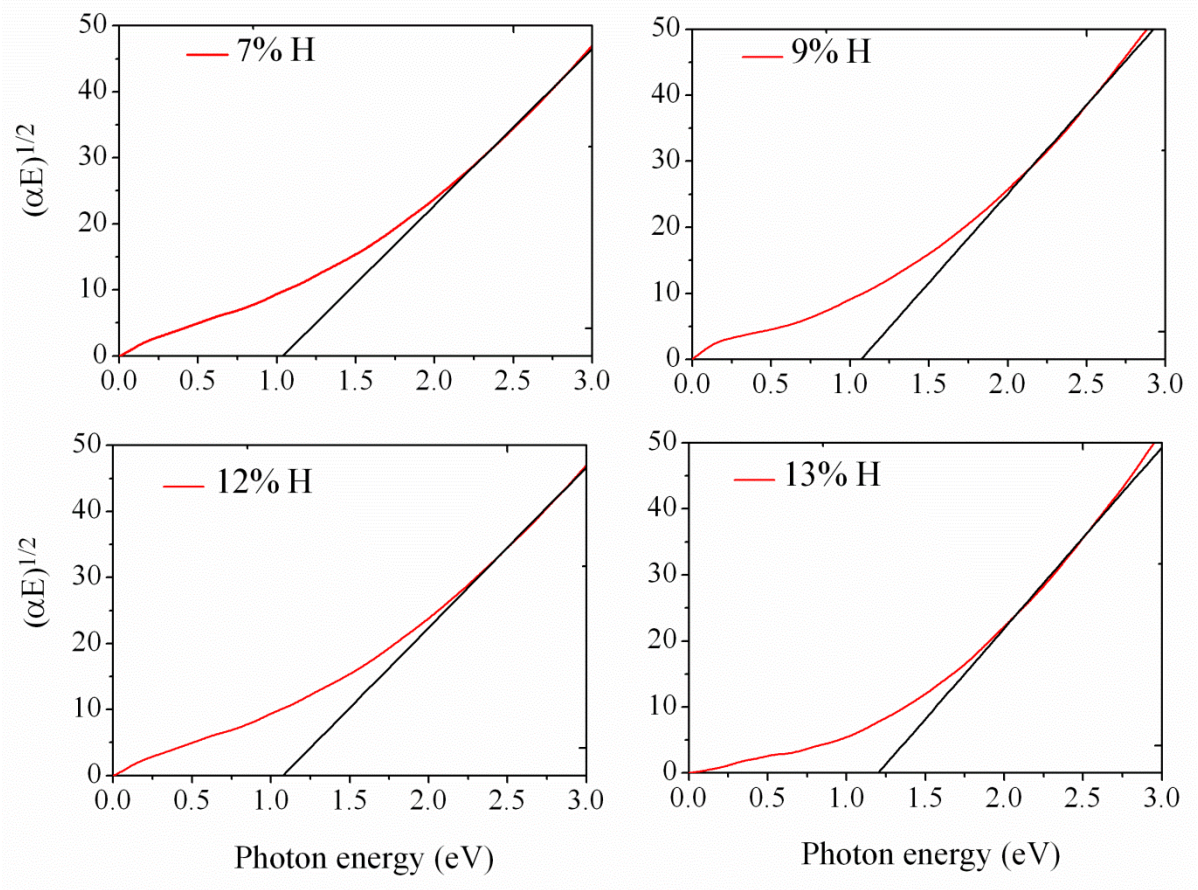

Fig. 5 Tauc plots to obtain the optical band gap for H under saturation in a-Si:H.

The experimental optical gap of device quality *a*-Si:H is in the range between 1.70 to 1.80 eV [53] and the impact of H content on the optical gap value in a-Si:H around H saturation has been already discussed in Ref. [14]. Considering a-Si:H at undersaturation, our Tauc plots give E_{opt} = 1.04, 1.09, 1.16 and 1.20 eV, as shown in Fig. 5 for H contents of 7, 9, 12 and 13% respectively, and E_{opt} = 0.92 eV for non-hydrogenated a-Si. As discussed in ref [14] the size of the change in the optical gap with H content is significant and is consistent with experimentally determined band gap changes [23-27]. Although GGA-DFT clearly underestimates the band gap of Si, the behaviour of our computed optical band gap as function of H content is in reasonable agreement with the experimental results [14, 23-27]. We are presently unable to perform hybrid DFT calculations of the optical gap of these structures, but present in section 3.2.2 and in ref. 14 some hybrid DFT results for the mobility gap, which gives extra confidence in the GGA-DFT results.

When we consider higher H concentrations, for which the Tauc plots are shown in Fig. 6, the extracted optical gaps are 1.25, 1.22 and 1.15 eV for 14%, 16% and 18% respectively. Here, we see that mild oversaturation with H in fact leads to a *reduction* in the optical gap of a-Si:H, as compared to saturated a-Si:H.

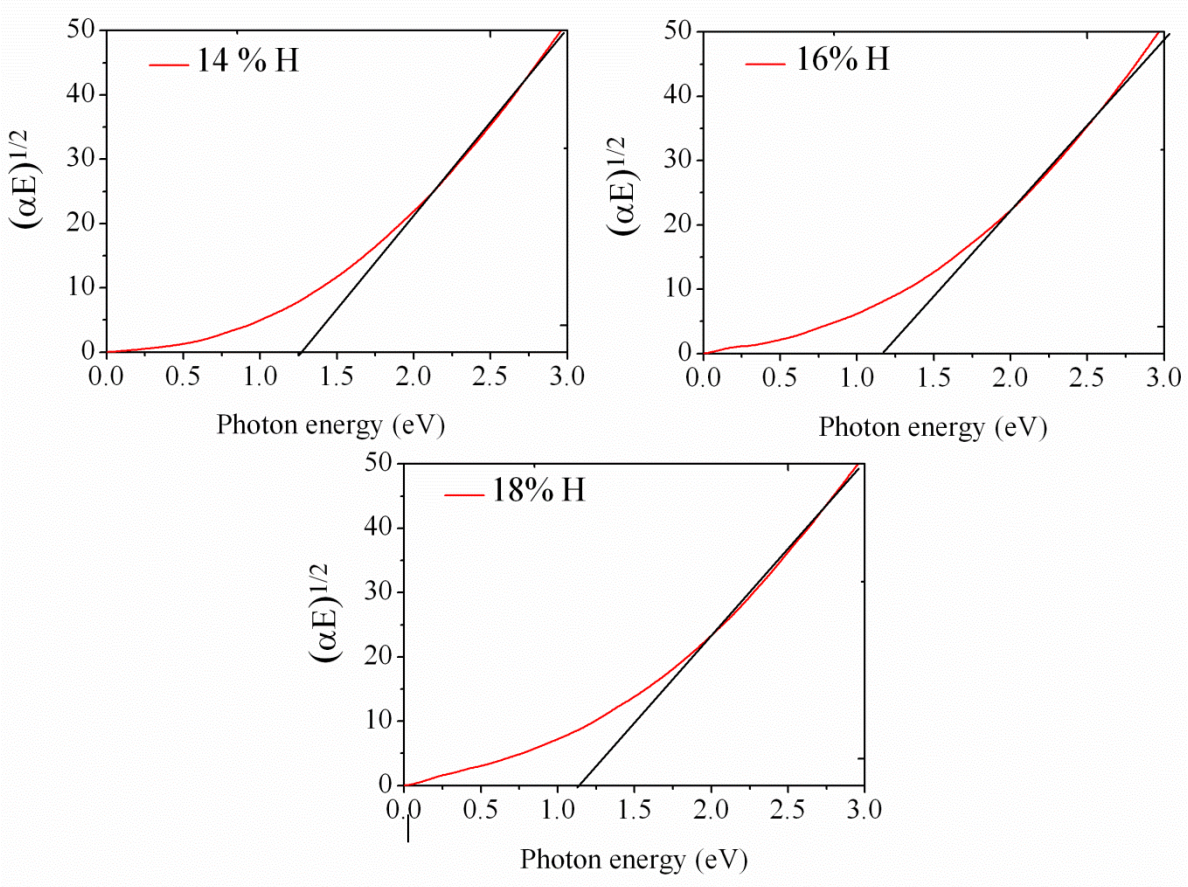

Fig. 6 Tauc plots to obtain the optical band gap of a-Si:H for H saturated (14%) and mildly oversaturation (16%, 18%).

3.2.2 Mobility Gap and Electronic properties of hydrogenated amorphous silicon.

The electron and hole wavefunctions that extend over the whole structure are characteristic for energy states- in which the charge carriers can be considered as free carriers. These states are non-localized and are called *extended states.* The wavefunctions of the tail and defect states are however localized in a small region of the structure and therefore these states are called *localized states.* It is difficult to identify an energy gap in the presence of coordination defects, since the effect of coordination defects on the electronic structure is to fill the gap with localized states whose energy is near the Fermi level, as discussed in Refs. [1, 2].

Consequently, the mobility that characterizes transport of carriers through the localized states in a-Si:H is strongly reduced. The term *mobility gap*, E_{mob}, is used because the presence of a considerable density of states in this gap conflicts the classical concept of band gap. The energy levels that separate the extended states from the localized states in a-Si:H are called the valence band and the conduction band mobility edges.

In order to quantitatively probe electron localization around the mobility edges, we calculate the inverse participation ratio (IPR) [5], of the wavefunction of each energy eigenstate, $\varphi_i(r)$, namely:

$$IPR_i = \mathrm{V}\frac{\int_v |\varphi_i(r)|^4\, dr}{\left[\int_v |\varphi(\mathrm{r})|^2\, dr\right]^2} \qquad (4)$$

where V is the volume of our supercell. This provides a good indication for the various topological and chemical defects that emerge in our structural models as the larger the IPR for an electronic state the more spatially localized it is.

To investigate how the electronic properties in the gap evolve with H content, we have calculate the IPR for undersaturated, saturated and mildly oversaturated H contents in a-Si:H. We have determined the individual atomic contributions to the total IPR for a localized eigenstate, to associate that state with particular structural irregularities. This provides a good indication for the various defect structures that emerge in our models. Since the important electronic states are those near to the Fermi level, our presentation deals only with the energy eigenvalues which are at mid-gap or near the band-tails of the spectrum.

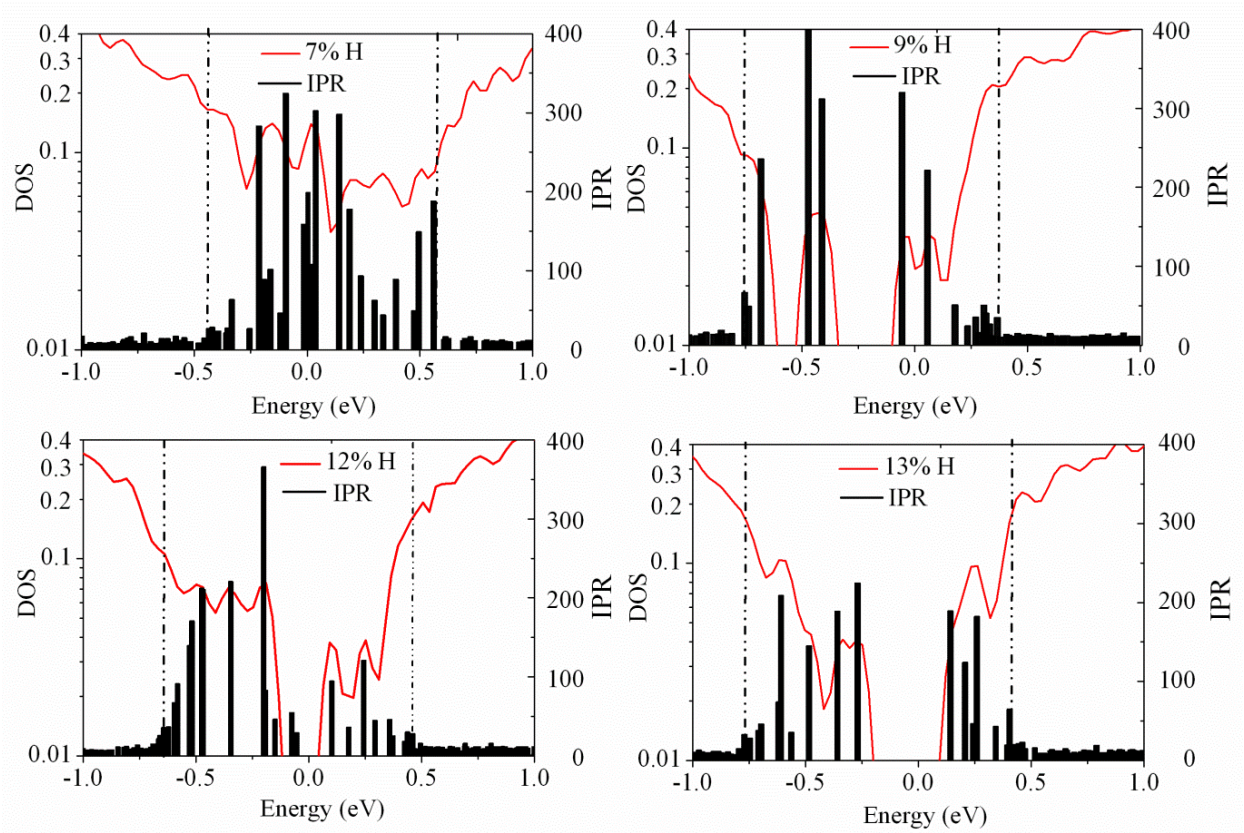

Fig. 7 Plots of semi-log density of states (red line) and Inverse Participation Ratio (IPR, histogram) for undersaturated (7%, 9% 12% and 13%) a-Si:H.

Fig. 7 shows the semi-log plot of density of states and IPR versus energy for under saturated a-Si:H. The density of electronic states around the Fermi level clearly decreases as the H concentration increases from 7 to 14%, which we will discuss further below. At 14% H concentration (fully saturated a-Si:H) the midgap states are removed, since this structure has neither dangling bonds nor extra H atoms implying midgap states are minimized. In Fig. 8 we also show the semi-log density of states and IPR for H concentrations of 16% and 18% H in a-Si:H. In the case of mild over saturation we find new states in the gap, which is consistent with the change in the optical gap with H oversaturation and will also be discussed below.

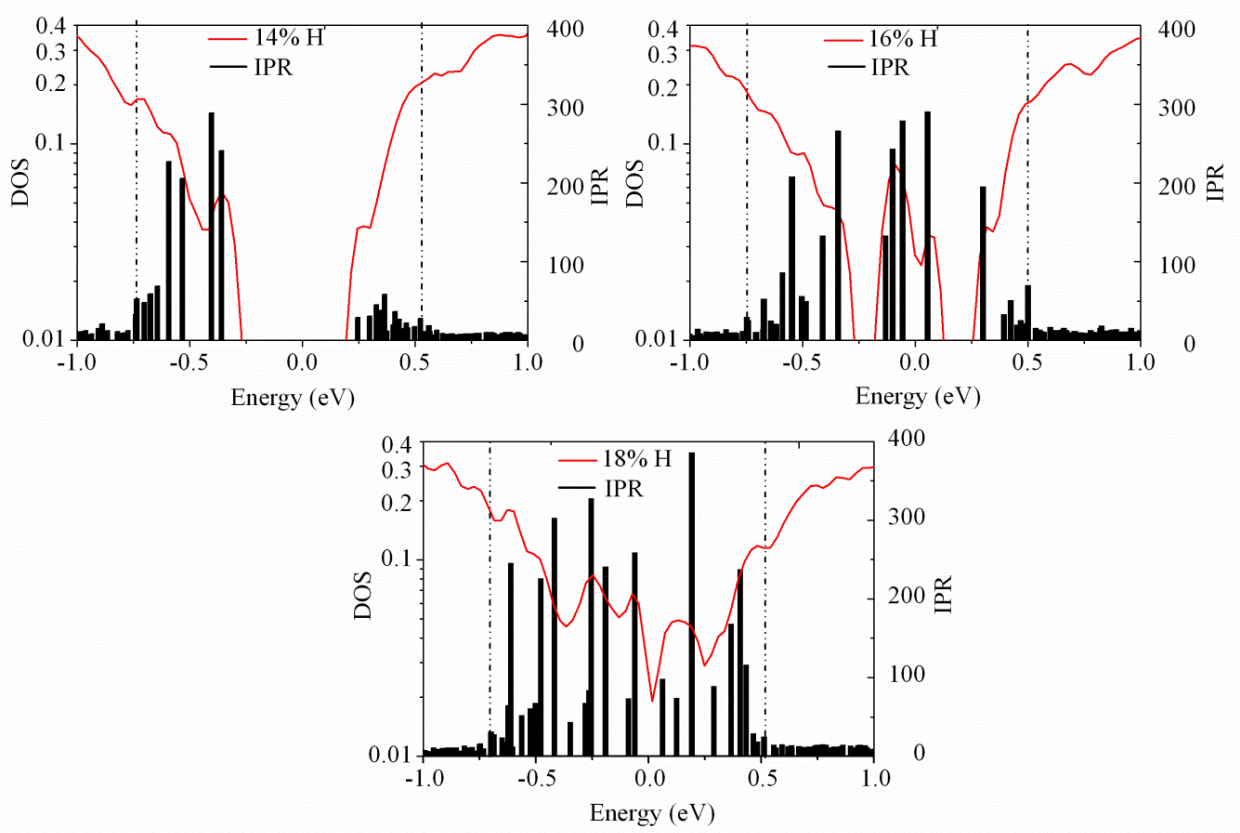

Fig. 8 Plots of semi-log density of states (red line) and Inverse Participation Ratio (IPR, histogram) for saturated (14%) and over saturated (16%, 18%) a-Si:H

We see that the IPR evolves with H content. For a-Si:H there are localized states around the band edges, arising from the well-known structural features present in a-Si:H, and these states appear around the Fermi level for both undersaturation and mild oversaturation. The computed mobility gaps, where the mobility edges are indicated in Figs. 7 and 8 are 1.03, 1.13, 1.16, 1.24, 1.27, 1.25 and 1.22 eV for 7%, 9%, 12%, 13% 14%, 16% and 18% H concentration, respectively.

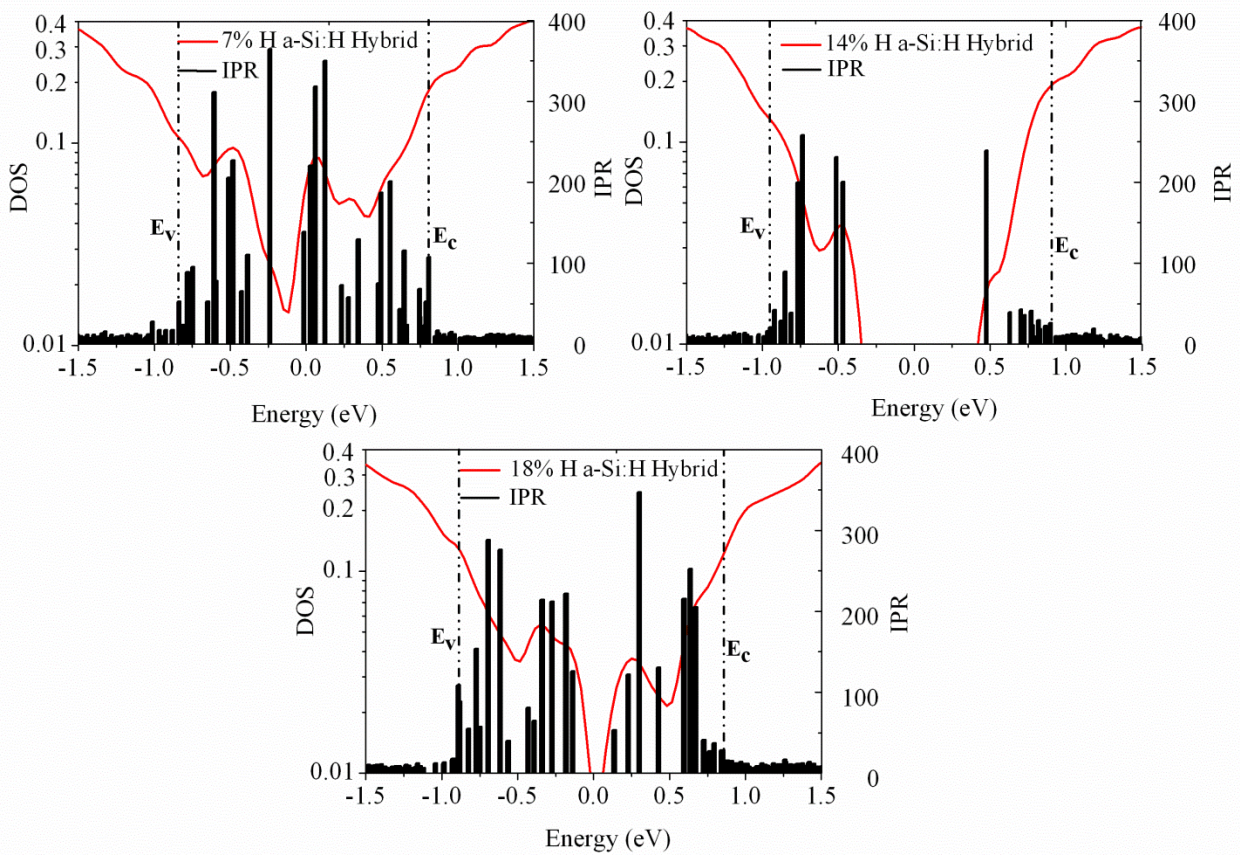

Fig. 9 Plots of semi-log density of states (red line) and Inverse Participation Ratio (IPR, histogram) versus energy from hybrid DFT (HSE06) for (a) under saturated (7%) (b) saturated (14%) and (c) oversaturated (18%) a-Si:H.

To examine the impact of the band gap underestimation with GGA-DFT, we plot in Fig. 9 the IPR from hybrid DFT for one H concentration in each regime of hydrogen content. The mobility gaps of a-Si:H with 7%, 14% and 18 % H concentrations are computed as 1.62, 1.83 and 1.76 eV. The hybrid DFT mobility gap has already been shown to be in very good agreement with experiment [14] and the behavior of mobility gap versus H content is consistent with the behavior obtained from the GGA-DFT calculations, giving confidence to our conclusions from GGA-DFT results.

The mobility and optical band gaps are plotted against the H concentration in a-Si:H in Fig. 10. Both have their maximum value for the saturated H concentration. The relationship

between the optical and mobility gaps and the H content is represented by a volcano-like curve, such that the optical and mobility gaps reach a maximum at H saturation. For the mobility gap, we compared the hybrid DFT mobility gap at one example in each regime of hydrogen concentration (undersaturated, saturated and mildly oversaturated) and comparison with the corresponding GGA-DFT mobility gap shows the consistency of the GGA-DFT findings regarding the behaviour of the mobility gap with hydrogen content. To the best of our knowledge, this result showing directly the evolution of the optical and mobility gaps in a-Si:H from H undersaturation to mild oversaturation has not been presented before.

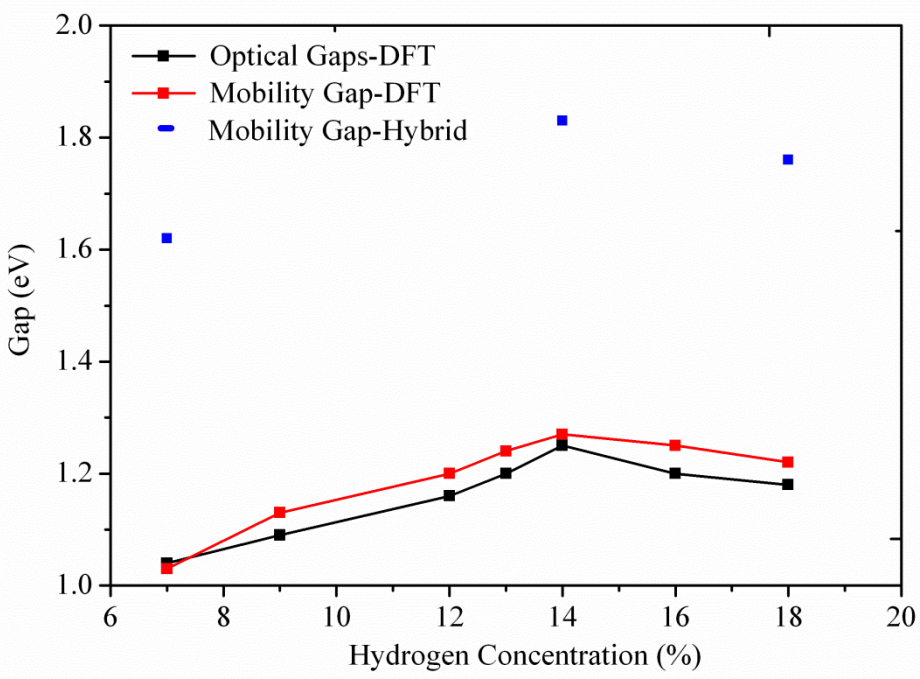

Fig. 10 Mobility and optical band gap energies as a function of H concentration in a-Si:H. The blue squares are the hybrid DFT values of the mobility gap.

To understand the behavior of optical and mobility gaps in a-Si:H as function of H concentration, in particular with mild H oversaturation, we examine in detail the electronic density of states (EDOS) and the local atomic structure. The total EDOS of a-Si:H is shown in Fig. 11 for different H contents. Examining the region around the Fermi level (set to 0 eV)

we see a zero EDOS in the case of H saturation (14%). Both for under (7%, 9% 12% and 13%) and over (16% and 18%) saturation there is a finite, non-zero EDOS around the Fermi level. The non-zero EDOS in the gap results in a reduction of the optical and mobility gaps and is consistent with the behaviour of the latter H content. The non-zero EDOS in the gap will also enhance charge recombination after light excitation and contribute to a degradation of solar cell performance [54].

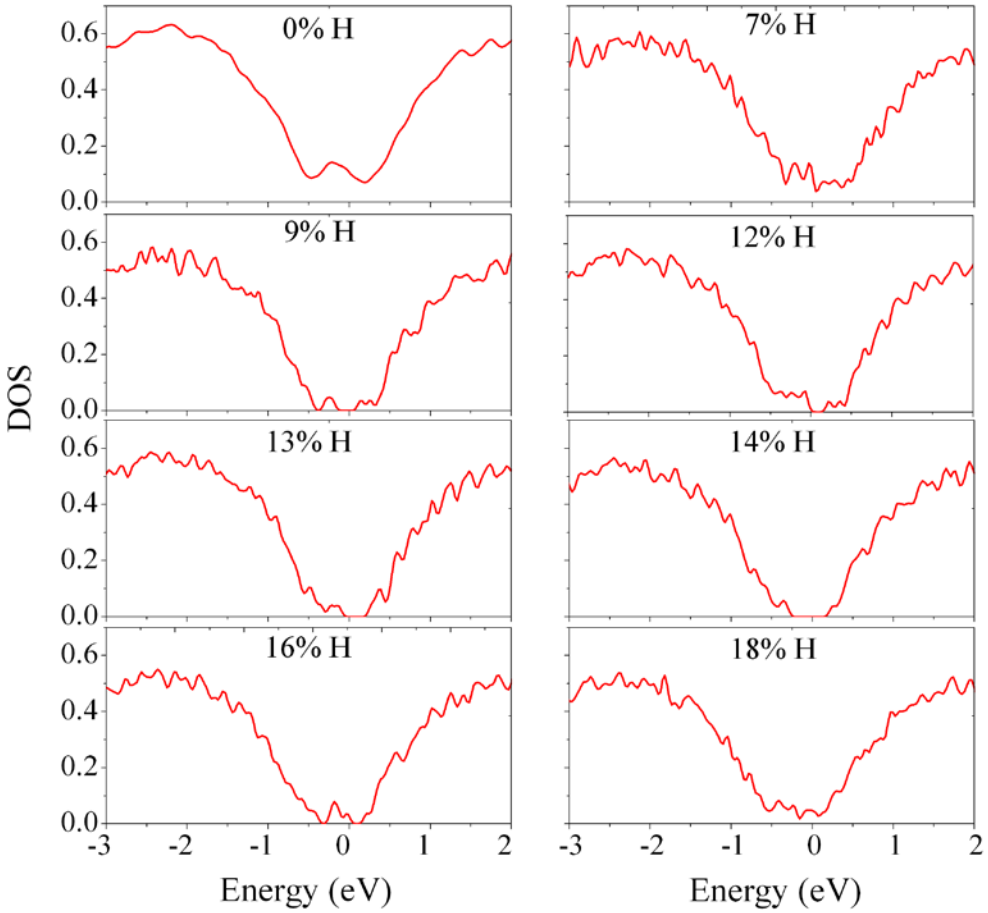

Fig. 11 Total DOS for a-Si:H with different H contents. The Fermi level is set to 0 eV.

For H undersaturation, the finite EDOS around the Fermi level arises primarily from the formation of dangling silicon bonds, as well as from elongated Si-Si bonds, as is discussed in the literature [20]. For the over saturation case the origin of the finite EDOS is not so

obvious, since there should be no dangling bonds in this system, so we seek another explanation.

We present a more detailed structural and electronic description of mildly oversaturated a-Si:H through analysis of the Si-Si bond length distribution, which is shown in Fig. 12 for a-Si and for different H concentrations. This distribution is calculated by defining the cut-off distance for a Si-Si bond up to the first minimum in the correlation functions of each sample. This distribution function shows a sharp peak at around 2.34 Å for all H contents, with a noticeable tail of longer Si-Si bonds. The Si-Si bond distribution of a-Si and a a-Si:H with a H content of 7% shows notable deviations from the perfect tetrahedral network and a bond length distribution that extends to Si-Si distances of about 2.70 Å. Dangling bonds have distances to their nearest non-bonded Si neighbor significantly longer than this (3.20 Å).

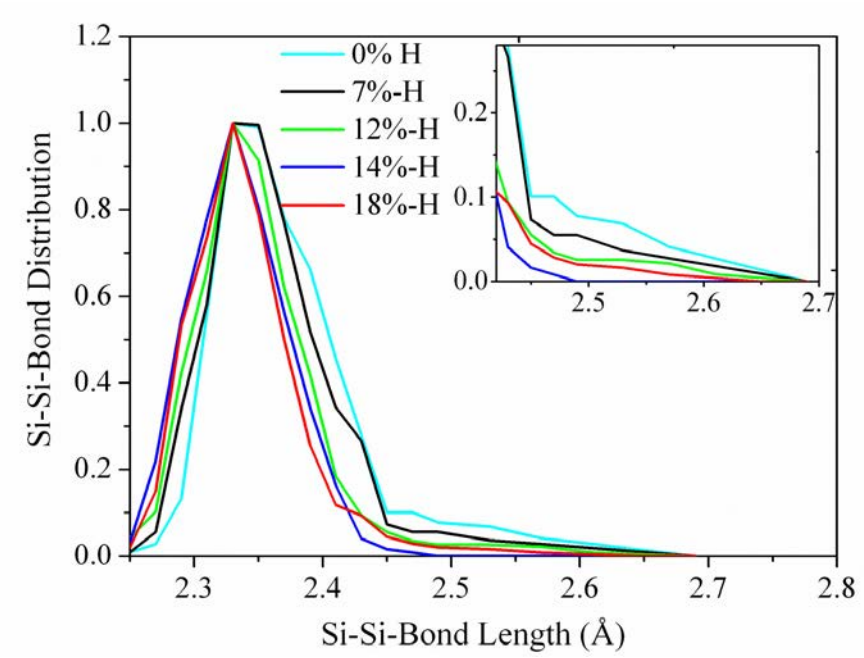

Fig. 12 Distribution of Si-Si-bond lengths for a-Si and a-Si:H with different H concentrations.

Focusing now on the variation of the long, or strained, Si-Si bonds with H content, we see that the presence of these bonds reduces as the H content increases up to saturation. At the same time, with the tail for saturated a-Si:H results the shortest of all our samples (see inset of Fig. 12). As the H content increases beyond saturation, there is a significant re-emergence of long Si-Si bonds, clearly visible in the tail of the distribution. Thus, as the H content increases beyond saturation, strained Si-Si bonds appear.

To examine the local atomic structure of the strained Si-Si bonds, we show in Fig. 13 a section of our a-Si:H structure with a H content of 18%. Here, silicon is indicated by yellow spheres, H by white spheres and the green spheres indicate H atoms that bridge neighboring silicon atoms. The bridging H and the two silicon it bridges can be clearly seen in Fig. 13. The formation of these Si-H-Si bridges generates 5-fold silicon atoms that have elongated Si-Si distances: from 2.40 Å at saturation to 2.64 Å at mild oversaturation. Therefore, this provides an origin for the mid-gap states in over saturated a-Si:H which we expand on below. This bridging H atom in oversaturated a-Si:H was also observed in the studies from Maroudas [29] and Stuckelberger et al. [55] even though different methods to prepare a-Si:H samples on have been used.

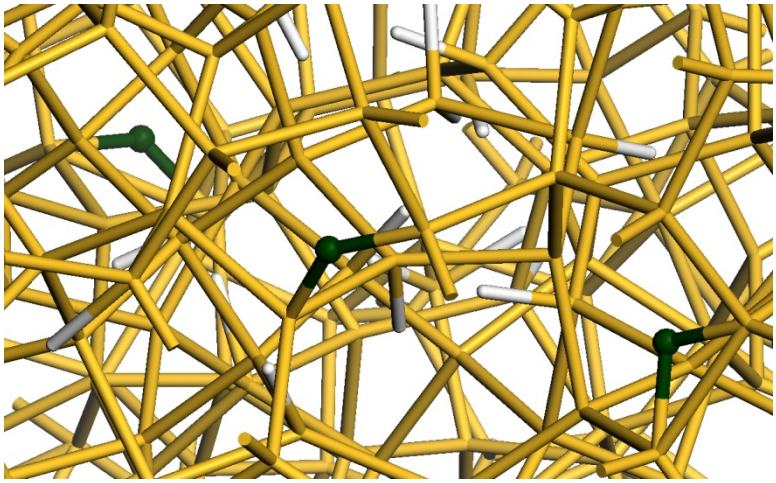

Fig. 13 Atomic structure of a section of the structural model for mildly oversaturated a-Si:H with a H content of 18%. Si are yellow spheres, H are white spheres and green spheres are also H atoms that make bridges between silicon atoms.

To further confirm the origin of the mid-gap states in oversaturated a-Si:H, the projected density of states of undersaturated (7%), saturated (14%) and oversaturated (18%) a-Si:H are shown in Fig. 14, for different types of Si atoms. These are Si-Si bonds shorter than equilibrium, Si-Si bonds longer than equilibrium and dangling Si bonds. For 14% and 18% H contents there are no dangling bonds present, so they cannot be the origin of the mid-gap states at mild oversaturation of H.

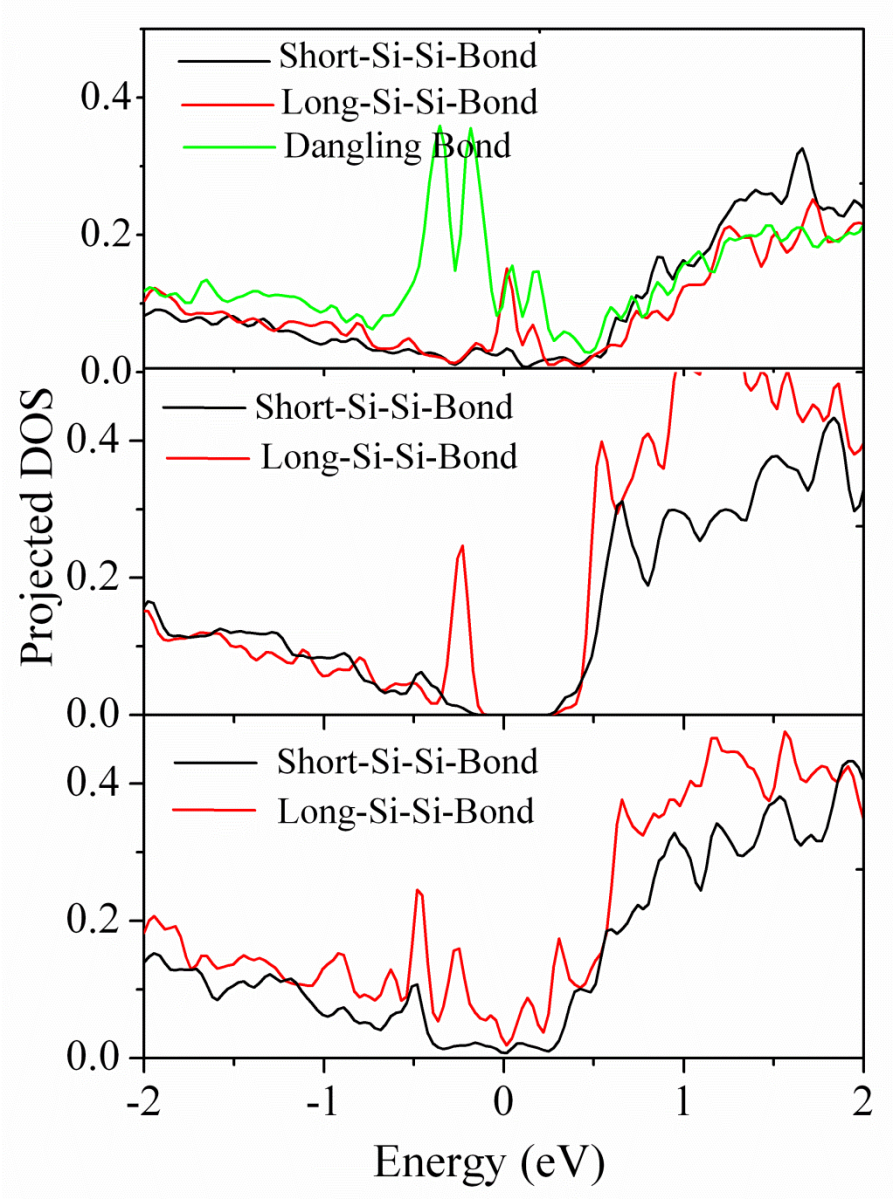

Fig. 14 Projected density of states of (a) unsaturated (7%), (b) saturated (14%) and (c) oversaturated (18%) of a-Si:H.

We see that the band edge states of undersaturated 7% a-Si:H have their origin in the dangling Si, but that the mid-gap states have strong contributions from the dangling Si and from strained (long) Si-Si bonds as the structure is saturated, consistent with the Si-Si bond distribution in Fig. 13. For hydrogen saturation (14%), the shorter and strained Si-Si bonds are insignificant the case of oversaturated a-Si:H, the mid-gap states are derived almost entirely from the strained Si-Si bonds which have arisen as a result of the incorporation of

extra H. The short Si-Si bonds make a minor contribution to the mid-gap EDOS. Thus, the importance of strained Si-Si bonds in a-Si:H for determining the optical and mobility gaps of a-Si:H is clear.

4. Concluding Remarks

We have used DFT calculations, both GGA-DFT and hybrid DFT, to show that a-Si:H exhibits a maximum in the optical and mobility gaps with H concentration, identifying the regimes of hydrogen undersaturation, saturation and a new regime we have termed *mild oversaturation*. The optical and mobility gaps show a volcano-like dependence as the H content is changed from 7% (undersaturation) to 18% (mild oversaturation). At the same time, mid-gap states associated with dangling Si and strained Si-Si bonds (bonds that are longer than the equilibrium Si-Si distance) disappear at saturation but states associated with strained Si-Si bonds reappear at mild oversaturation, in consistent with the evolution of the optical gap.

Standard structural analyses of our models are unable to provide a detailed description of the influence of H content. However, an examination of the distribution of Si-Si bond distances provides the key to the change in electronic properties. In the H-undersaturation case, the new electronic states in the gap arise from the presence of dangling and strained Si-Si bonds. Increased H concentration up to saturation reduces the strained bonds and removes dangling bonds. In the case of mild oversaturation the mid-gap states arise exclusively from an increase in the density of strained Si-Si bonds. Analysis of our structures shows that, in addition, a fraction of the extra H atoms form a bridge between neighboring silicon atoms and increase the Si-Si distance and promoting bond length disorder in the sample.

While it is outside the scope of this work to examine directly the effect of hydrogen content on light induced degradation in the Staebler-Wronski (SW) effect, we can make some remarks on how our results may relate to efforts to understand this important effect in a-Si:H. A supported model of the SW effect in a-Si:H is one in which the irradiation with light breaks weak strained Si-Si bonds, which creates unpassivated dangling Si or Si vacancies, both of which are involved in the formation of gap states that reduce the performance of an a-Si:H solar cell. In the present paper, we find that strained Si-Si bonds are present in both undersaturated and mildly oversaturated a-Si:H and we propose that if Si-H bonds and strained Si-Si bonds are broken and Si (di-)vacancies would form, then in undersaturated a-Si:H this will lead to undercoordinated dangling silicon. In contrast, the excess hydrogen in our mildly oversaturated samples will not form as many undercoordinated dangling silicon as the extra hydrogen will be able to passivate more dangling silicon or Si vacancies, thus reducing the severity of the SW effect. At the same time, the excess of hydrogen does reduce the band gap over the case of hydrogen saturation (figure 10) but this may be less of an issue if light-induced degradation is reduced. It would therefore be of great interest to design experiments that would probe the validity of this proposition.

Acknowledgements

We acknowledge support from The European Commission, through the 7th Framework ICT-FET-Proactive program, Project: SiNAPS (contract no 257856) and MN acknowledges the Science Foundation Ireland (SFI) Starting Investigator Research Grant Program, project "EMOIN" grant number SFI 09/SIRG/I1620. We also acknowledge computing resources provided by SFI to the Tyndall National Institute and by the SFI and Higher Education Authority Funded Irish Centre for High End Computing.

References

[1] R. A. Street Hydrogenated Amorphous Silicon, Cambridge University Press, Cambridge, UK (2005).

[2] T. Searle, Properties of Amorphous Silicon and its Alloys (EMSI Data Reviews, No. 19), Institute of Electrical Engineers, UK, (1998)

[3] Y. Kuo, Thin Film Transistors: Materials and Processes, 1st Edition, Springer (2003)

[4] R. A. Street, Thin Film Transistors, Adv. Mat., 21 2007 (2009).

[5] J. Ziman, Models of Disorder, Cambridge Univ. Press, Cambridge, (1979).

[6] A. G. Hamers, M. N. van den Donker, B. Stannowski, R. Schatmann, and G. J. Jongerden, Plasma Process. Polym. 4, 275 (2007).

[7] A. V. Shah, R. Platz, and H. Keppner, Sol. Energy Mater. Sol. Cells 38, 501 (1995).

[8] D. L. Staebler, and C. M. Wronski, Appl. Phys. Lett. 31, 292 (1977).

[9] A. H. M. Smets, W. M. M. Kessels, and M. C. M. van de Sanden, Appl. Phys. Lett. 82, 1547–1549 (2003).

[10] A. Smets, C. Wronski, M. Zeman, and M. van de Sanden," Mater. Res. Soc. Symp. Proc., San Francisco, CA (Materials Research Society, 2010), Vol. 1245, p. 1245–A14-02.

[11] S. Zhang and H. Branz, Phys. Rev. Lett. 87, 105503 (2001).

[12] M. Fehr, A. Schnegg, B. Rech, O. Astakhov, F. Finger, R. Bittl, C. Teutloff, and K. Lips, Phys. Rev. Lett., 112, 066403 (2014)

[13] H. Tanimoto, H. Arai, H. Mizubayashi, M. Yamanaka and I. Sakata, J. Appl. Phys. 115, 073503 (2014)

[14] M. Legesse, M. Nolan and G. Fagas, J. Phys. Chem. C, 117, 23956 (2013).

[15] P. A. Fedders, D. A. Drabold, and S. Nakhmanson, Phys. Rev. B 58, 15624 (1998).

[16] J. Dong, and D. A. Drabold, Phys. Rev. Lett. 80, 1928 (1998).

[17] Y. Pan, F. Inam, M. Zhang, D. A. Drabold, Phys. Rev. Lett. 100, 206403 (2008).

[18] B. Biswas, C. Z. Wang, C. T Chan, K. M. Ho, and C. M. Soukoulis, Phys. Rev. Lett. 63, 14 (1989).

[19] B. G. Yacobi, Semiconductor materials, Kluwer academic publishers, New York, (2003).

[20] P. A. Khomyakov, W. Andreoni, N. D. Afify, and A. Curioni, Phys. Rev. Lett. 107, 255502 (2011).

[21] S. Yamasaki, Phil Mag B, 56, 70 (1987).

[22] M. Yamaguchi, and K. Morigaki, Phil. Mag. B, 79, 387 (1999).

[23] M. Daouahi, A. Ben Othmane, K. Zellama, A. Zeinert, M. Essamet, and H. Bouchriha, Solid State Comm 120, 243 (2001)

[24] R. N. Kre, M. L. Mousse, Y. Tchetche, F. X. D. Bouo Bella, and P. A. Thomas, Int. J. Phys. Sci. 5, 675 (2010)

[25] C. Manfredotti, F. Fizzotti, M. Boero, P. Pastorino, P. Polesello, and E. Vittone, Phys. Rev. B, 50, 18046 (1994)

[26] Viturro, R. E & Wieser, K., Phil. Mag. B 53, 93-103 (1986).

[27] G. D. Cody, T. Tiedje, B. Abeles, B. Brooks, and Y. Goldstein, Phys. Rev. Lett. 47, 1480 (1981).

[28] S. Ramalingam, D. Maroudas, and E. S. Aydil, J. Appl. Phys., 86, 2872 (1999)

[29] S. Sriraman, S. Agarwal, S. A. Aydil, and D. Maroudas, Nature, 418, 62 (2002)

[30] S. Sriraman, M. S. Valipa, E. S. Aydil, and D. Maroudas, J. Appl. Phys., 100, 053514 (2006)

[31] J. Tersoff, Phys. Rev. B 39, 5566 (1989)

[32] C. Krzeminski, Q. Brulin, V. Cuny, E. Lecat, E. Lampin, and F. Cleri, J. Appl. Phys. 101, 123506 (2007).

[33] F. Hao, D. Fang, and Z. Xu, Appl. Phys. Lett. 100, 091903 (2012)

[34] J. D. Gale and A. L. Rohl, Molecular Simulation, 29, 291 (2003).

[35] F. Wooten, K. Wiener, and D. Weaire, Phys. Rev. Lett. 54, 1392 (1985).

[36] R. Car, and M. Parrinello, Phys. Rev. Lett. 60, 204 (1988).

[37] N. C. Cooper, C. M. Goringe, and D. R. McKenzie, Comp. Mater. Sci. 17, 1 (2000).

[38] W. Kohn and L. J. Sham, Phys. Rev. 140, A1133 (1965).

[39] G. Kresse, and J. Furthmüller, Phys. Rev. B 54, 11169 (1996).

[40] J. P. Perdew, J. A. Chevary, S. H. Vosko K. A. Jackson, M. A. Pedersen, and D. J. Singh, Phys. Rev. B 46, 6671 (1992).

[41] G. Kresse, and D. Joubert, Phys. Rev. B 59, 1758 (1999).

[42] H. J. Monkhorst, and J. D. Pack, Phys. Rev. B, 13, 5188 (1976).

[43] J. Paier, M. Marsman, K. Hummer, G. Kresse, I. C. Gerber and J. G. Ángyán, J. Chem. Phys., 124, 154709 (2006).

[44] G. Lucovsky, R. J. Nemanich, and J. C. Knight, Phys. Rev. B 19 2064 (1979).

[45] T. Matsui, H. Sai, K. Saito, M. Kondo Jpn. J. Appl. Phys., 51, p. 10NB04 (2012).

[46] K. Laaziri, S. Kycia, S. Roorda, M. Chicione, J. L. Roberston, J. Wang, and S. C. Moss, Phys. Rev. B 60, 13520 (1999)

[47] K. Laaziri, S. Kycia, S. Roorda, M. Chicione, J. L. Roberston, J. Wang, and S. C. Moss, Phys. Rev. Lett., 82, 3460 (1999).

[48] W. A. Kamitakahara, H. R. Shanks, J. F. McClelland, U. Buchenau, F. Gompf, and L. Pintschovius, Phys. Rev. Lett. 52, 644 (1984).

[49] R. Biswas, A. M. Bouchard, W. A. Kamitakahara, G. S. Grest, and C. M. Soukoulis, Phys. Rev. Lett. 60, 2280 (1988).

[50] P. Biswas, and D. A. Drabold, Phys. Rev. B 76, 125210/1-125210/5 (2007).

[51] K. Jarolimek, R. A. de Groot, G. A. de Wijs, and M. Zeman, Phys. Rev. B 79, 155206 (2009).

[52] J. Furthmueller, VASP postprocessing code. Downloaded from www.freeware.vasp.de. (accessed 25 September 2012).

[53] S. Lee, J. K. Arch, S. J. Fonahs, C. R. Wronski, Photovoltasics Specialists Conference, doi:10.1109/pvsc.1990.111884; C. M. Wronski, S. Lee, M. Hicks, and S. Kumar, Phys. Rev. Lett. 63, 1420 (1989).

[54] M. Stutzmann, W. B. Jackson, and C. C. Tsai, Phys. Rev. B32, 23 (1985).

[55] M. Stuckelberger, M. Despeisse, G. Bugnon, J.-W. Schüttauf, F. J. Haug, C. Ballif, J. Appl. Phys., 114, 154509 (2013).